

# Construction of Multiple-Beam Optical Traps with Nanometer-Resolution Position Sensing

Koen Visscher, Steven P. Gross, and Steven M. Block

(Invited Paper)

**Abstract**— We describe the design and construction of two different types of multiple-beam optical tweezers, each equipped with nanometer-resolution position detectors. Multiple optical traps can be created either by splitting a laser beam in two parts, based on its polarization, or time-sharing a single beam among several different locations. The advantages and disadvantages of optical tweezers based on either scheme are discussed, along with details of specific implementations. Various ways to detect microscopic movements of an optically trapped object are presented and compared, including designs that are relatively insensitive to absolute location of a trapped particle within the field of view. Two of many possible applications for such instruments are illustrated: the detection of molecular steps by kinesin motor molecules, and determinations of the stiffness of single microtubules.

## I. INTRODUCTION

AS OUR understanding of biological systems has deepened, there has been concomitant interest in understanding processes at the molecular level. Traditional approaches, such as genetics, indicate which biomolecules are important for particular phenomena, but seldom point to a physical mechanism for their action. Structural approaches supply static images of these biomolecules and additional clues as to mechanism, but provide an incomplete picture of dynamic processes. A new tool, optical trapping (or “optical tweezers”), made by focusing a laser beam to a diffraction-limited spot [1]–[4], provides a means to generate and measure molecular-scale forces for the study of individual biomolecules, allowing experimentalists to perform physiology at the macromolecular level. Already, researchers have begun to use this tool to probe molecular details of such diverse activities as vesicle transport, muscle contraction, and RNA transcription. Optical tweezers have proved especially important in the study of molecular motors, proteins that convert chemical energy, usually in the form of ATP, into force and displacement along polymeric tracks, such as actin filaments or microtubules [5]–[7]. A wide variety of motor proteins exists in nature, each with distinct properties and functions: those of the myosin family move on actin and are responsible for muscle contraction, as well as

cytokinesis and certain types of vesicle motion; those of the kinesin and dynein families move on microtubules and are responsible for the beating of cilia and flagella, the separation of chromosomes during cell division, and for additional types of vesicle motion. Other classes of enzymes exhibit motor-like properties as they translocate on nucleic acids and may also be considered “motor proteins,” although they are not typically classified as such. These include the polymerases and ribosomes, which are responsible for carrying out replication, transcription, and translation of DNA and RNA.

Optical trapping microscopes specifically designed for work with single-molecule assays should have the following desirable features.

- 1) Imaging should be done at high magnification and with the greatest possible resolution, which requires the use of high numerical aperture (NA), oil- or water-immersion objectives and condensers. Particularly useful imaging modes include epi-fluorescence, effective in imaging single actin filaments, and/or video-enhanced, differential interference contrast (DIC) microscopy, effective in imaging single microtubules.
- 2) The microscope should be equipped with one or more optical traps, each capable of independent motion within the field of view. These “tweezers” serve two roles: a) they permit indirect manipulation of single molecules by means of attached beads
- 3) , and b) they greatly reduce the Brownian (thermal) motion of trapped beads, making possible rapid measurements with nanometer resolution.
- 4) Sensitive position detectors for objects trapped by the system are required. A wide temporal bandwidth is desirable for such detectors (>10 kHz), especially for calibration of optical trap stiffness (see below).
- 5) Combining optical tweezers with position detectors enables the development of feedback systems to create either isometric “position” clamps (used to keep the position of the trapped particle constant) or isotonic “force” clamps (used to keep the force on a trapped particle constant).

Microscope systems designed for nanometer-level measurement are extremely sensitive to both mechanical and acoustic vibrations, and must be mounted on air isolation tables. In addition, it helps to place such systems in environments with low acoustic noise, for example, inside sound-proofed enclosures.

Manuscript received October 11, 1996; revised January 6, 1997. The work of S.P. Gross and S. M. Block was supported by grants from the National Institutes of Health.

The authors are with the Department of Molecular Biology, Princeton University, Princeton, NJ 08544 USA.

Publisher Item Identifier S 1077-260X(96)09638-4.

## II. OPTICAL TWEEZERS AND STIFFNESS

Dielectric particles in a laser beam are subject to at least two distinct types of optical force: a scattering force, acting in the direction of propagation of the light on the particle, and a gradient force, due to the interaction of dipoles with the electric field gradient that exists in the laser beam [1]. A laser beam is focused to a diffraction-limited spot by a lens of high numerical aperture, to produce a significant spatial gradient. Near the focal zone, the gradient force is sufficient to overcome the scattering force, and small dielectric particles are pulled toward the region of high light intensity [1]: this is optical tweezers. Stable, three-dimensional (3-D) trapping of micrometer-sized objects in water, including both latex beads and biological material (such as bacteria and organelles), has been demonstrated [1]–[4], [8]. Living specimens absorb light most weakly in the near infrared, so trapping lasers used for biological work are typically in the wavelength region of 800–1100 nm, to minimize photodamage. Forces exerted on trapped particles are in the piconewton (pN) range. For small displacements from the center of an optical trap, the restoring force is proportional to displacement, which means that optical tweezers acts like a Hookeian spring, characterized by a fixed stiffness. In most of our experiments, we are interested mainly in the lateral stiffness, i.e., stiffness in the plane of the specimen. The stiffness depends on the wavelength and power of the laser used, as well as the size and refractive index of the particle, and the refractive index of the surrounding medium [1]. In combination with high-resolution position sensors, the optical tweezers can be used to make quantitative measurements of both the positions of trapped objects and the forces applied to them, once the stiffness is calibrated. Theoretical prediction of trapping forces is not easy, because the equations describing light scattering in strongly convergent electromagnetic fields are difficult to solve [9]. However, any of several well-established methods may be used to determine trapping forces empirically, each with its own attendant advantages and disadvantages.

### A. Escape Force Method

This method determines the minimal force required to pull an object free of the trap entirely, generally accomplished by imposing a viscous drag force whose magnitude can be computed [4], [8]. Historically, this was the first method proposed and used to estimate optical trapping forces [1]. To produce the necessary force, the particle may either be pulled through the fluid (by moving the trap relative to a stationary stage), or more conventionally, the fluid can be moved past the particle (by moving the stage relative to a stationary trap). Many variations of the method exist: one of the simplest is to videotape a trapped particle in a fixed trap while translating the microscope stage (e.g., by hand) at an ever-increasing rate, until the particle just escapes. The particle velocity immediately after escape is measured from the video record, which permits an estimate of the escape force, provided that the viscous drag coefficient of the particle is known. While somewhat crude, this technique permits calibration of force to within about 10%. If the stage is instead moved at a

fixed, known velocity, the laser trapping power can be reduced until the particle just escapes, which provides somewhat better reproducibility of measurements. Note that escape forces are determined by optical properties at the very edges of the trap, where the restoring force is no longer a linear function of the displacement [10]. Since the measurement is not at the center of the trap, the trap stiffness cannot be ascertained. Escape forces are generally somewhat different in the  $x$ ,  $y$ , and  $z$  directions, so the exact escape path must be determined for precise measurements. This calibration method does not require a position detector with nanometer resolution.

### B. Drag Force Method

By applying a known viscous drag force,  $F$ , and measuring the displacement produced from the trap center,  $x$ , the stiffness  $\alpha$  follows from  $\alpha = F/x$ . In practice, drag forces are usually produced by periodic movement of the microscope stage while holding the particle in a fixed trap: either triangle waves of displacement (corresponding to a square wave of force) or sine waves of displacement (corresponding to cosine waves of force) work well [9], [11]–[13]. Once trap stiffness is determined, optical forces can be computed from knowledge of the particle position relative to the trap center, provided that measurements are made within the linear (Hookeian) region of the trap. Apart from the need for a well-calibrated piezo stage and position detector, the viscous drag on the particle must be known. This can be problematic, since drag coefficients depend on the size and shape of particles, the viscosity of the fluid, and the possible presence of nearby walls or obstacles. They are generally unknown for irregularly shaped particles. The method is therefore best suited to uniform spherical particles, for which explicit expressions for the drag exist, even near chamber walls [9]. For example, the drag increases by 40% or more when a sphere approaches a wall within a distance equal to its radius, and by  $\sim 200\%$  within a quarter radius. Work at such short distances can pose serious problems, but see Wang *et al.* [13], where the strong distance dependence of the drag near a wall was turned to an advantage by using it to calibrate the height of trapped sphere to within  $\pm 50$  nm.

### C. Equipartition Method

One of the simplest and most straightforward ways of determining trap stiffness,  $\alpha$ , is to measure the thermal fluctuations in position of a trapped particle. The stiffness of the tweezers is then computed from the Equipartition theorem for a particle bound in a harmonic potential:  $\frac{1}{2}kT = \frac{1}{2}\alpha\langle x^2 \rangle$ , where  $kT$  is Boltzmann's constant times the absolute temperature. The chief advantage of this method is that knowledge of the viscous drag coefficient is not required (and therefore of the particle's geometry as well as the fluid viscosity). A fast, well-calibrated position detector is essential, precluding video-based schemes. Although knowledge of particle size, shape, and optical properties is not necessary, it should be borne in mind that these properties will affect detector calibration. When using this method, there are two cautions: first, the analog bandwidth of the detection system must be considerable, since any lowpass filtering will underestimate  $\langle x^2 \rangle$  and inflate

the apparent stiffness. Second,  $\langle x^2 \rangle$  is a statistically biased estimator: any other systematic sources of noise (electronic noise, drift, etc.) will artificially inflate  $\langle x^2 \rangle$  and underestimate the stiffness. Finally, thermal motion represents a weighted average over positions near the center of the trap (in a way that depends on the trap stiffness), and care must be taken so that the optical potential remains harmonic over the region explored by this motion. Although the analog bandwidth of the position detector must remain high, for the reasons just discussed, one feature of the Equipartition method is that the digital sampling rate at which the position of the object is updated need not be correspondingly high, i.e., possible aliasing artifacts are not a consideration, since the position signal has random phase.

#### D. Power Spectrum Method

A third method, quite accurate when the particle's viscous drag coefficient,  $\beta$ , is known, is based on the determining the power spectrum of the position of a trapped object. For a particle bound in a harmonic potential at low Reynolds' number (i.e., when inertia can be neglected), the position  $x$  is described by the differential equation  $\beta \dot{x}(t) + \alpha x(t) = F(t)$ , where  $F(t)$  is a Langevin force. Solving for  $\tilde{X}(f)$ , the Fourier transform of  $x(t)$ , and applying the Equipartition Theorem yields  $kT/\alpha = \langle x^2 \rangle = 2\pi \int_0^\infty \tilde{X}(f)\tilde{X}^*(f)df$ , and the power spectrum for position is a Lorentzian given by  $\tilde{X}(f)\tilde{X}^*(f) = kTf_c/\alpha\pi^2(f^2 + f_c^2)$ , which has a roll-off frequency  $f_c = \alpha/2\pi\beta$ . The trap stiffness may be determined from this roll-off frequency by fitting the spectrum to a Lorentzian. Fig. 1 shows a typical power spectrum for the position of a 0.5- $\mu\text{m}$  silica bead held by optical tweezers in water. The use of power spectra to calibrate trap stiffness can be particularly helpful in exposing potential problems with optical tweezers. If the tweezers are misaligned, the beam is corrupted, or something is awry with the position detection system, then the power spectrum rapidly becomes non-Lorentzian and/or displays peaks at specific noise frequencies. These details can be readily missed with other methods. Because only the roll-off frequency needs to be determined, the power spectrum may have arbitrary amplitude scaling, so that absolute calibration of the position sensor is unnecessary. When an absolute calibration is available, the value of the power spectrum at zero frequency also provides identical information to the previous method. Essentially identical considerations about analog bandwidth apply here as for the previous method.

#### E. Step Response Method

The trap stiffness may also be determined by finding the response of a particle to a rapid, stepwise movement of the trap [12]. For small steps of the trap,  $x_t$ , the response,  $x_b$ , is given by  $x_b = x_t(1 - \exp(-\alpha t/\beta))$ . To determine the trap stiffness  $\alpha$ , the viscous drag,  $\beta$ , must be known. Here again, a calibrated detector is not required. As with some of the other methods, care must be taken so that the particle remains within the linear region of the trap. Although it provides essentially the same information as the power spectral method, above, it is far harder to identify extraneous sources of noise or artifact

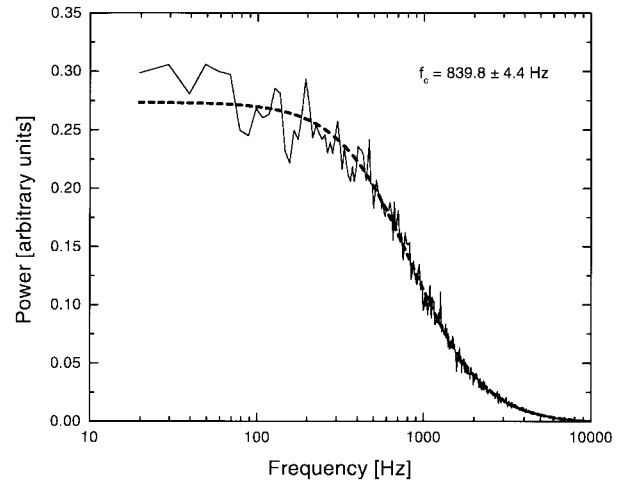


Fig. 1. Power spectrum for the position of an optically trapped silica bead (0.5- $\mu\text{m}$  diameter). The Lorentzian shape of the power spectrum (data: solid line; fit curve: dashed line) is characteristic of a bead trapped in equilibrium with a well-aligned trap. The roll-off frequency,  $f_c$ , obtained by fitting the spectrum, may be used to determine trap stiffness ( $\sim 0.025$  pN/nm, here).

using this approach. The time constant for movement of the trap must be faster than the characteristic damping time of the particle,  $\beta/\alpha$ , and essentially identical considerations about analog bandwidth apply here as for the previous two methods.

With the exception of the method described in Section II-C, all approaches essentially measure the ratio of the stiffness to the damping and therefore require some independent way of estimating the viscous drag contribution. The methods described in Sections II-D and II-E are perhaps better suited to signal averaging than some of the others and therefore statistically quite robust. The methods described in Sections II-A and II-B are particularly well suited to mapping the force profile of traps in the outermost nonlinear regions [9]. While it is true that some of the methods do not use absolute detector calibration to determine trap stiffness, this calibration may nevertheless be required once stiffness is known, for force computations. Note that all these approaches are analogous to methods of system identification used for linear filters in analog electronic circuits: the equivalent circuit for a trapped particle is a first-order lowpass filter (e.g., an RC filter). The method in Section II-D, for example, is equivalent to computing output power spectrum of a filter with Gaussian white noise input, while the method in Section II-E measures the filter response to a Heaviside step function.

### III. MULTIPLE OPTICAL TWEEZERS

Certain experiments, like red blood cell deformability studies [14], single myosin molecule assays [5], [6], or microtubule stiffness measurements [15], [16], can benefit from the use of two or more optical traps to establish the experimental geometry. Multiple tweezers can be constructed trivially by increasing the number of laser light sources, a simple but costly solution. If only two traps are desired, however, a single laser beam can be split in two, based on polarization [17]. In either case, the beams forming all the traps are simultaneously present in the specimen. A more flexible way of creating multiple tweezers from a single light source is

to time-share the laser beam among a set of positions in the specimen plane [18], by rapidly scanning its position back and forth among these (analogous to the way separate traces are created in a multiple-beam oscilloscope). If the light is scanned quickly enough, the rapidly “blinking” individual traps mimic the effect of steady illumination (see below). Multiple-beam tweezers can be technically challenging to construct, due to a requirement for fast, exceptionally well-controlled beam deflections, with nanometer-level reproducibility. This, in turn, places significant demands on the pointing stability of the laser source and scanning hardware.

Fig. 2 demonstrates the use of a multiple-beam trap, where 10 silica beads ( $0.5\text{-}\mu\text{m}$  diameter) are trapped individually in a circular pattern of time-shared optical traps. Two orthogonal acoustooptical deflectors (AOD’s) were used to scan the tweezers. Because the AOD’s are computer controlled, the number and relative strengths of the traps, their spatial patterns, as well as the scanning rates can all be chosen with great flexibility, without the need to change any optics. Instead of creating discrete traps by pausing the beam at desired locations, continuous streaks of moving light can also be generated, creating line-like traps. To demonstrate this approach, Sasaki *et al.* [19] trapped large numbers of microspheres inside a micrometer-scale pattern corresponding the Japanese character for light, *hikari*. The choice of trap design is influenced by cost, the desired degree of flexibility, required power, and difficulty of construction. Both a dual-beam laser trap and a time-shared trap are currently in use in our lab and will be discussed below. For our work, multiple traps need to be moved relative to one another in an independent fashion, and so alternative designs that rely on multiple-beam interference effects [20] or holographically generated structures have not been considered. However, such approaches may soon become feasible with the advent of electronically controlled microoptics.

There are two basic ways to construct a position- or force-feedback system: dynamically modulate either the laser power [13], [21] or the beam position [5], [6], [12]. Because it already incorporates all the technology necessary to move the laser beam, a time-shared trap is exceptionally well suited to the latter approach. In a position-clamping arrangement, the feedback signal for displacement can be used to measure an externally applied force. Such a time-shared setup was used by Molloy *et al.* to study molecular forces produced by the myosin protein [6].

#### A. Trap Stiffness in Multiple Tweezers

An important characteristic of optical tweezers is the trap stiffness, which sets the restoring force that can be applied to objects, as well as the time scale of their motion. Many issues of trap design therefore focus on stiffness considerations. In the dual-beam trap, both beams are simultaneously present, so the stiffness of each of the independent tweezers is determined directly by the optical power in each laser beam. The beams have orthogonal polarization, and there is little interference when the two tweezers are brought into close proximity, although some residual interference can occur, due to depolarization effects arising from the use of high-numerical-aperture optics.

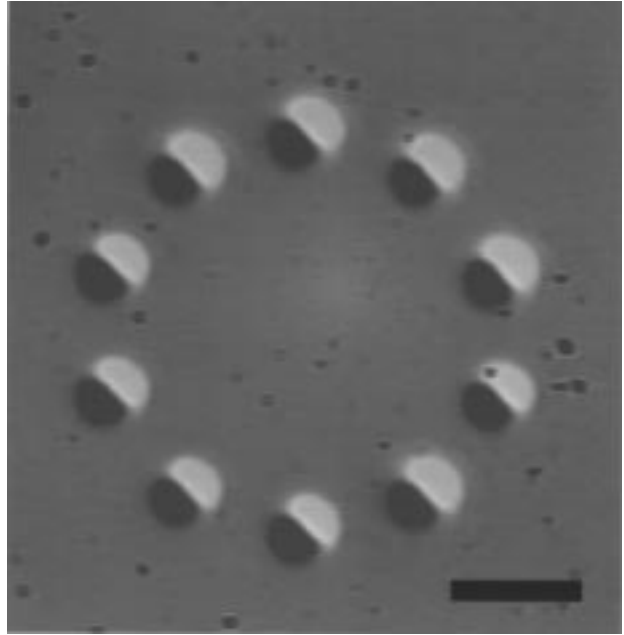


Fig. 2. Demonstration of a time-shared, multiple-beam optical trap. Ten silica beads ( $0.5\text{-}\mu\text{m}$  diameter) are trapped in a circular pattern produced by a single beam whose computer-controlled position alternates rapidly among the ten separate locations. Scale bar,  $2\ \mu\text{m}$ .

While time-sharing systems offer improved flexibility, this comes at a price: the effective stiffness of each of the alternating tweezers is correspondingly diminished because of the reduced duty cycle. The frequency response of a trapped particle falls off rapidly at frequencies greater than  $f_c$  (Fig. 1), hence its motion becomes insensitive to external disturbances much faster than  $1/f_c$ . When  $N$  time-shared tweezers are produced from a single laser beam, we scan at rates well above the roll-off frequency, so that the individual trap stiffness drops to  $\alpha/N$ , where  $\alpha$  is the stiffness of a single-trap configuration. When the scanning frequency is comparable to or below  $f_c$ , the stiffness of each synthesized trap effectively becomes time-varying, which can lead to problems in measurement. In our system, a 20-kHz trap scanning rate was implemented, which is considerably faster than typical roll-off frequencies of micrometer-sized spheres (250–1500 Hz): the scan rate is limited by software and hardware considerations, discussed later.

Responses of nonspherical structures to optical trapping forces are more difficult to calculate. Consider, for example, a dumbbell-shaped object, consisting of two trapped beads connected by a thin, flexible linkage with stiffness  $\alpha_l$ , each held in one of two different alternating traps with stiffness  $\kappa = \alpha/2$ . Such an object approximates the experimental geometry found in experiments on myosin, where two beads are joined by a single actin filament [5], [6]. How must time-shared tweezers be used to generate tension in the linkage? The effective stiffness of the system along the axis of the linkage is  $\alpha_{\text{eff}} = \kappa + (\kappa\alpha_l/(\kappa + \alpha_l))$ , so  $\alpha_{\text{eff}}$  varies from  $\alpha/2$  to  $\alpha$  as  $\alpha_l$  goes from zero to infinity. For compliant linkages, the effective stiffness corresponds to that of one (alternating) trap, while for an inextensible linkage, the traps work in parallel and the total stiffness is the sum of each of the trap stiffnesses. Provided that the scan frequency remains well above the maximum roll-

off frequency (set by the sum of these trap stiffnesses), one can generate tension in the linkage by moving the tweezers somewhat apart. Speed, therefore, is a major consideration in selecting a scanning device for the time-sharing tweezers. We consider three alternative means of beam deflection.

### B. Scanning Galvanometer Mirrors

The step response times for these devices can be as low as 0.3–1 ms, fast enough to produce two alternating traps with comparatively low roll-off frequencies  $\sim 200$ – $300$  Hz). However, the wobble, jitter, and repeatability figures for galvanometer mirrors may not be good enough to achieve nanometer-level positional stability in the specimen plane of a microscope. Because deflection devices are randomly accessed in multiple-beam traps, the use of faster resonant scanning mirrors would seem to be precluded. However, feedback stabilization schemes, based on nanometer-scale detection of the position of the trapping beams, may make possible some specialized applications of galvanometer mirrors. Their principal advantages include very large deflection angles, negligible optical power losses, and lower cost.

### C. Electrooptic Deflectors

In an electrooptic deflector (EOD), the light is deflected by a linear refractive index gradient created in an electrooptical material by an applied electric field. The deflection angle is  $\theta \propto LV/a^2$ , where  $L$  is the length of the cell,  $V$  is the applied voltage, and  $a$  is the aperture diameter. In contrast to AOD's, the undeflected beam goes straight through the device, making optical alignment straightforward. The optical throughput can be as high as 90% and is limited only by small reflection and absorption and scattering losses. The EOD switching time is  $\sim 100$  ns (limited mainly by the capacitive load), far faster than galvanometer mirrors, and even beyond most AOD's. Beam-pointing stability, which depends chiefly on noise levels in the supply voltage, should be ample for nanometer-level stability. However, the small maximum angle of deflection achieved by most EOD's (2-mrad full angle) results in a maximum separation of only  $\sim 1$   $\mu\text{m}$  between traps, which may be inadequate for many applications. Wavefront distortion caused by crystal imperfections can also be a problem.

### D. Acoustooptic Deflectors

In an AOD, first-order diffracted light is generated by sending the laser beam through a density grating in a crystal, created by a traveling acoustic wave at ultrasound frequencies. The deflection angle of the first order light is given by  $\theta = \lambda f/v$ , where  $\lambda$  is the wavelength,  $f$  is the acoustic wave frequency, and  $v$  is the velocity of the sound wave. This angle, and therefore the tweezers' position, is determined by the acoustic frequency driving the crystal. For the device we use, that frequency ranges from 21 to 31 MHz, corresponding to 17-mrad full angle deflection. This permits a maximum trap separation of  $\sim 10$   $\mu\text{m}$  in the specimen plane. Because the diffraction efficiency in most AOD's is comparatively low ( $\sim 80\%$ , max), placing two orthogonally mounted devices in series to achieve both  $x$  and  $y$  deflections results in a

loss of  $>36\%$  of the incoming light. An additional drawback to AOD's is that their diffraction efficiency tends to change over the acoustic bandwidth, hence transmitted light levels (and therefore trap stiffness) can differ by as much as 10%–15% for different deflections. Although manufacturers tend to quote higher peak transmittance figures than 80%, these are not generally obtained over the complete range of deflections. Analog voltage-controlled oscillators typically used to drive the AOD's are not usually stable enough to achieve the desired beam-pointing stability: for applications requiring nanometer-level stability/repeatability, 24- or 32-b digital frequency synthesizers are needed. The response time of an AOD is intrinsically limited by the ratio of the acoustic velocity to the laser beam diameter:  $t_c = a/v$  (typically,  $t_c \sim 1.6$   $\mu\text{s}/\text{mm}$  of laser beam diameter). In practice, however, such times are not achieved by our setup; instead, the bus addressing speed of the computer-based digital frequency synthesizer limits the response bandwidth limit of our system to  $\sim 20$  kHz (corresponding to  $\sim 50$   $\mu\text{s}$ ).

## IV. POSITION DETECTION

Nanometer-resolution position detectors are an essential feature of optical traps used for single-molecule research, and several schemes have been developed. The most straightforward is to measure a particle's position is by directly imaging it onto the surface of a quadrant (or split) photodiode, after magnification by the microscope [5], [6], [22]. Photodiodes are generally used in a differential configuration, with the four quadrants being used pairwise for  $x$  and  $y$  sensing. Difference signals derived from both halves of such detectors are typically normalized by their sum to remove any dependence of the output on the total light level; this can be done either in hardware or software. In most cases, trapped particles are imaged by a conventional light source unrelated to the laser used for trapping, e.g., by the microscope's own tungsten-halogen illuminator. Systems with independent light sources for illumination and trapping are well suited to feedback-enhanced and/or time-sharing tweezers, because position signals are derived solely from the objects' position, with no contributions from the trap itself. Because an imaging photodiode detector system is fixed in space, however, the trapped object must be carefully aligned with the corresponding position of the detector at an appropriate place in the specimen plane.

In the past, bright field microscopy has been used to detect bead motion, but this produces reduced-contrast images and comparatively low light levels at the detector, in comparison with the laser-based methods described next. Shot noise typically limits the bandwidth of such systems to well below 1 kHz, but the situation can be improved somewhat by exchanging the tungsten-halogen light source for a higher luminosity xenon (or mercury) arc lamp [6], [12], although arc sources are less stable. Alternatively, laser light—at a different wavelength from the trapping source, e.g., in the visible—can provide increased flux at the photodetector. However, when used to supply light over an extended region, coherent laser sources produce their own set of problems arising from speckle and interference, necessitating some form of phase randomiza-

tion. This randomization must be accomplished at frequencies higher than the position-detector bandwidth.

Larger temporal bandwidths can readily be achieved if the trapping laser light is also used for particle detection. At least several milliwatts of laser power are required in the specimen plane to produce a stable trap. If even a small fraction of this light were used to measure position ( $\sim 1$  mW), the detector would not become noise-limited until quite high frequencies (tens of kilohertz), and faster detection could be achieved than using conventional sources. Following this line of thinking, a number of implementations have been developed which we will briefly describe. The first, and arguably most sensitive detector, is the optical trapping interferometer [7], [10], [23]. In this arrangement, a Wollaston prism located behind the objective in a microscope set up for DIC imaging splits the laser light into two orthogonally polarized beams, producing two overlapping, diffraction-limited spots in the specimen plane; together, these function as a single optical trap. After passing through the specimen, the beams are recombined behind the condenser in a second Wollaston prism. When no object is in the trap, or when a bead is exactly centered in the trap, the recombined beam has the same linear polarization as the incoming laser light. However, as the bead moves from the center of the trap, one beam is phase-delayed with respect to the other, such that after recombination, an elliptical polarization is produced. The degree of ellipticity, which can be measured quite sensitively, provides a direct measure of displacement. This detection scheme is intrinsically aligned, in the sense that both the trapping and photodetection beams are one and the same. In addition to its sensitivity, an advantage to this approach is that it is a nonimaging method; as such, the trap can be moved about within the specimen plane without the need to realign the position detection system. On the other hand, the optical tweezers and position detection cannot be spatially uncoupled, which precludes implementing a feedback system based on trap deflection. Moreover, this detection scheme is strictly one-dimensional: only displacements along the Wollaston shear axis are registered.

Other methods that use the trapping light for position detection vary in the type of photodiode used and its position on the optical path. The method implemented by Ghislain and Webb [24], [25] is based on a single photodiode sensor. This scheme was specifically designed to detect axial ( $z$ ) movements of objects, in contrast to most sensors, which detect lateral movement. A bead or particle, trapped just below the focus, is considered to act as a lens. As the bead moves from the trap center, it deflects the laser beam. The microscope condenser (or alternatively, a second objective), magnifies this beam and casts the transmitted light onto the surface of the photodiode: the magnification functions as an optical lever arm to facilitate measurement of small deflections. In contrast to the imaging system described earlier, the photodiode is not placed in an optical plane conjugate to the specimen (i.e., an image plane), where the particle would remain in focus. Instead, the location of the detector is chosen such that roughly half the optical power in the diverging cone of light illuminating it is intercepted (i.e., it was overfilled by a factor of  $\sim 2$ ). At this position, it turns out that axial (as well as lateral) displacements

are sensitively registered. Such a system is optimized for the detection of lateral motion when the active area of the detector is physically offset from the optical axis by about one detector radius [25]. Axial movements of a trapped particle cause the size of the light cone to change, and the resulting variation in intercepted power provides a measure of vertical displacement. Lateral displacements are also registered, through a change in overlap of the diode and the deflected light pattern, but no information about the  $x$ - $y$  direction can be obtained. Axial and lateral displacements cannot be deconvoluted in this simple setup, but this should be possible if a quadrant photodiode were used.

Another scheme that takes advantage of the trapping light to detect position was developed by Smith *et al.* [26], who positioned a lateral effect position detector in such a way that it captured all the transmitted light from the laser beam passing through the specimen. The transmitted power and associated beam deflection induced by the trapped object permits a computation of the total rate of change in beam momentum, which (by Newton's Laws) equals the force exerted on the particle. This approach, therefore, allows optical trapping forces to be measured without knowledge of trap stiffness or viscous drag or the geometry of the particle. For this work, two counterpropagating beams were used to form the trap, and the deflection of one was monitored to determine force. In a two-beam counterpropagating trap, the laser light need not be as sharply focused as in a single-beam gradient trap, and therefore the back aperture of the objective need not be filled with light. Underfilling this aperture guarantees that all of the deflected light can be captured at the condenser side, permitting direct computation of the force. Unfortunately, this method is not readily adapted to single-beam gradient force traps, because the objective aperture must be fully filled (or even overfilled) to achieve axial stability.

To measure nanometer-scale displacements in the two systems described below, we used an alternate scheme. Laser light passing through the specimen is collected on a quadrant photodiode placed on the optical axis in a position that is optically conjugate to the back focal plane of the microscope condenser. In contrast to the scheme employed by Ghislain and Webb [24], [25], the active area of our photodiode detector is somewhat larger than that of the illuminating beam, which renders it nearly insensitive to axial ( $z$ ) movements. Moreover, the detector is centered on the optical axis. By locating the detector at this particular position, it turns out that its response is rendered insensitive to the  $x$ - $y$  position of the optical trap itself within the specimen plane: instead, it responds mainly to a *relative* displacement between an object and the center of the trap, wherever that trap is located (in practice, within an area  $\sim 5$   $\mu\text{m}$  or so in diameter). The principles of operation of this scheme are illustrated in Fig. 3. This ability to register displacements in a manner that remains nearly independent of trap location is the principal advantage of this scheme over other photodiode-imaging methods (and is a property that it shares with the optical trapping interferometer described previously). In practice, one cannot assure the exact geometry of Fig. 3, where the beam is perfectly collimated by the trapped bead. Trap position-independent responses can nevertheless be

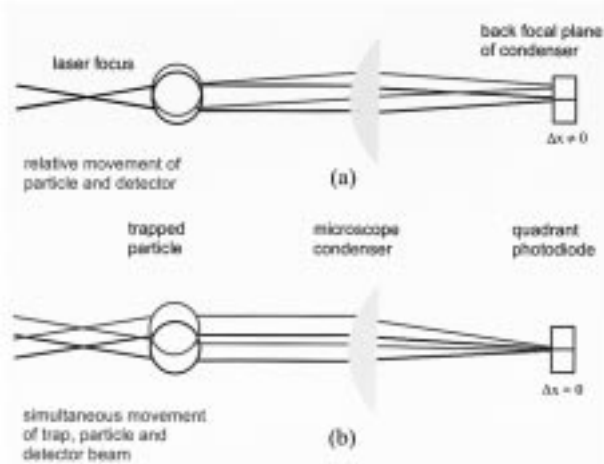


Fig. 3. The principle of the position detection scheme used. The position detector is placed on the optical axis at a plane conjugate to the back focal plane of the condenser. In this ray-optic approximation, the trapped bead acts as a simple lens. (a) A signal change, corresponding to a physical displacement in the light beam at the split photodiode detector (red versus black rays, right) is generated when the bead moves relative to the stationary detector beam. (b) However, no corresponding change in the signal is produced when both the bead and detector beam are moved together by the same amount. At this optical position, the detector response is nearly insensitive to the absolute location of the detector beam within the microscope field of view, but is instead sensitive only to relative movements of the object and detector beam.

achieved for a given particle by adjusting the axial position of the sensor while moving both the optical trap and the particle together, until the detector signal is nulled. For multiple-beam traps or feedback-enhanced systems, uncoupling the trapping and illuminating light sources becomes necessary. For this purpose, a second laser source at a different wavelength (and lower power) may equally well be focused to a diffraction-limited spot, overlapped with the location of a trapping beam in the specimen plane, and used for position detection, taking the identical approach.

How do these detection methods compare when it comes to mechanical vibrations or pointing fluctuations of the light source? Direct-imaging methods are particularly sensitive to mechanical vibrations in the arm of the apparatus holding the detector, although they are comparatively insensitive to vibrations in the illumination arm. The optical trapping interferometer is relatively insensitive to vibrations of the condenser arm of the microscope (since only the state of polarization is evaluated) and therefore does not require any special mechanical reinforcement. Conversely, it is extremely vulnerable to fluctuations in the position of the trap relative to the particle, and special precautions, such as single-mode fiber coupling, [7] may be required to improve laser-pointing stability. Methods that rely on the lens-like properties of the particle in the trap will generally be sensitive to both laser-pointing instabilities and vibrations of the detector.

## V. DESCRIPTION OF THE INSTRUMENTS

### A. The Dual-Beam Trap

Our dual-beam trap is based on an inverted microscope (Axiovert 100, Zeiss) equipped with high NA, DIC optics.

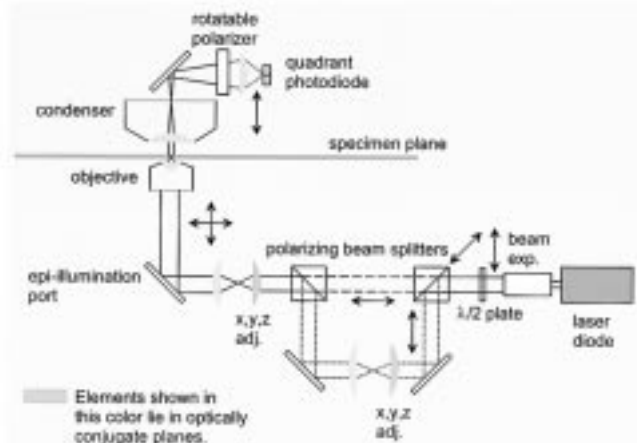


Fig. 4. Schematic of the dual-beam trap. The polarization state of the beam is indicated by the arrows and line type (short dash: vertical polarization; long dash: horizontal polarization). The rear lenses of two 1:1 telescopes are each mounted on  $x$ - $y$ - $z$  translation stages and arranged to deflect the trapping light: one moves the two traps jointly, the other moves one separately. Rotation of the polarizer located directly in front of the quadrant photodiode controls which trapping beam is transmitted for position detection.

A CCD camera (C2400, Hamamatsu) relays video signals to an image processor (Argus 20, Hamamatsu), whose output is recorded by a VCR. Fig. 4 shows a diagram of the optical path. A polarized beam of light from a diode laser (200-mW 830-nm Melles Griot) is expanded threefold and passed through a rotatable halfwave plate. Turning this waveplate alters the power split between two orthogonally polarized trapping beams, produced by a polarizing beam-splitting cube. The beam reflected by the cube (short dashed line) is passed through a pair of lenses that form a 1:1 telescope. The first of these lenses can be moved by translation stages in the  $x$ ,  $y$ , and  $z$  directions and is used to adjust the position of one optical trap relative to the other. Following the telescope, the beam is recombined with the beam transmitted by the first cube (long dashed line) in a second polarizing beam-splitting cube. The combined beams pass through a second 1:1 telescope, again equipped with a movable first lens. This telescope adjusts jointly the position of both optical traps. Both rear telescope lenses (colored blue) are arranged in such a way that they are imaged into the back aperture of the objective; this insures that lens movements scan the optical trap with minimal aberration and constant power in the specimen plane. The combined laser beams are introduced into the microscope by means of a dichroic mirror located directly below the objective Wollaston prism. In the current setup, the light enters the microscope through the epi-illumination port, replacing the position normally occupied by the fluorescence cube. An objective (100X/1.3 NA oil Plan Neofluar, Zeiss) focuses the laser beams to diffraction-limited spots.

### B. The Position Detector

Either of the two trapping beams can be used for position detection. Both beams pass through the specimen (where they trap different objects, at different spatial locations) and into the condenser (1.4 NA, oil), after which they are deflected

from the microscope optical path by a  $45^\circ$  dichroic mirror mounted inside a tube holding the condenser. After emerging from the microscope, one of the two beams is blocked by a rotatable Glan–Thompson prism, while the unblocked beam (short dashed line) is transmitted to a photodiode (SPOT-9DM1, UDT) located in a plane that is optically conjugate to the back focal plane of the condenser (see above). The rotational orientation of the prism determines which beam is blocked. In principle, a fast-switching polarizer (e.g., a photoelastic modulator) could be used to alternately block the beams, allowing the simultaneous measurement of both bead positions. Although there is some depolarization induced by the high-NA optics and light scattering by the beads, the power at the detector from the transmitted beam is  $\sim$  thirty-fold larger than that of the blocked beam. A narrow-bandpass optical filter placed directly in front of the photodiode eliminates background light from other sources. Signals from the quadrants of the photodiode are amplified by a custom-built, two-stage preamplifier, and digitized by a 12-b multifunction A/D board (AT-MIO-16-E2, National Instruments). The approximate analog bandwidth of this system is 10 kHz.

### C. Detector Calibration

Calibration of trap stiffness and photodiode response is a three-stage process.

- 1) The pixel size of the video system is first determined by imaging a precision, diamond-ruled grid carrying a line pattern with  $10\text{-}\mu\text{m}$  spacing (Donsanto Corp.) on the CCD camera.
- 2) A piezo stage is then calibrated by driving it with a triangle-wave voltage and recording on video the movement of a bead fixed to the coverglass [27]. Due to piezo hysteresis and nonlinearity, this produces a nonlinear displacement waveform.
- 3) After calibration and linearization of the piezo stage [7], a bead fixed to the coverglass is moved through the trap with a periodic voltage computed to generate a true triangle-wave of displacement, while the detector response to this calibrated displacement is recorded.

### D. The Time-Sharing Trap

Two independent laser sources are used: the optical path for the time-sharing tweezers is shown in red, while the separate detection beam is shown in green (Fig. 5). The system is based on an inverted microscope (Diaphot 200, Nikon) equipped with high NA, DIC optics. Images are recorded with a monochrome CCD camera (XC-77RR, Sony). The trapping source is a diode-pumped, Nd:YVO<sub>4</sub> solid-state laser (Topaz, 1064 nm, 3 W CW, Spectra Physics), which is optically pumped by a 35-ft-long fiber bundle and requires no water or fan cooling; the laser head can therefore be mounted directly to the optical table carrying the microscope without introducing vibration. The laser power supply, which produces acoustic noise, is located outside of the soundproofed experimental chamber. The beam-pointing stability of this laser is sufficiently good that coupling to a single-mode fiber [7] has not

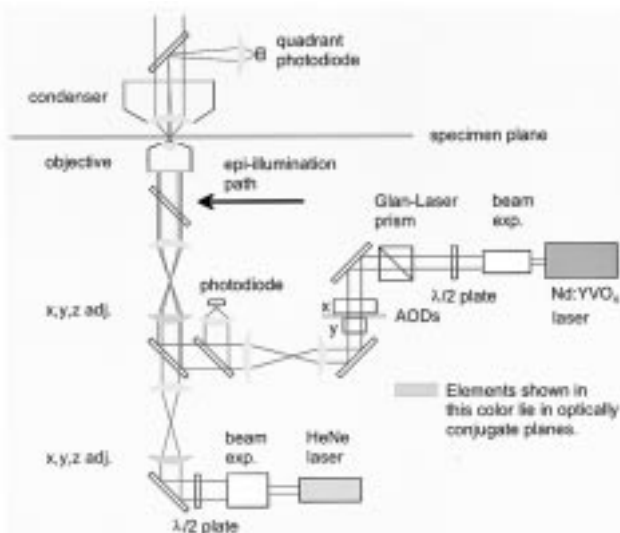


Fig. 5. Schematic of time-sharing optical tweezers. Light from a near-infrared laser (red lines) forms multiple optical traps after computer-controlled deflection by the AOD's. Light from a red laser (green lines) is used for position detection. As in Fig. 4, telescope lenses provide manual controls for the locations of the laser spots in the specimen plane. Objects colored blue are located in planes conjugate to the back aperture of the objective.

proved necessary to achieve nanometer-level resolution. The laser beam is first expanded (5X, CVI) to reduce divergence and obviate the need for major expansion after the AOD's (expansion at that stage reduces the deflection angle and thus the maximum trap separation achieved in the specimen). An attenuator (a combination rotatable  $\lambda/2$  plate and Glan-laser prism) is used to control laser power, after which the beam is deflected in  $x$  and  $y$  directions by two orthogonally mounted AOD's (model ATD-274HA16, IntraAction). The AOD drive voltage is generated in a PC-based 32-b digital frequency synthesizer board (model CVE-272A1, IntraAction), enabling computer-controlled trap movement. The first-order diffracted light is then expanded slightly to fill the back aperture of the objective. A beam sampler directs a small fraction of the laser light to a photodiode (PDA-50, Thorlabs) to monitor power in the diffracted order. After this, the beam is deflected by a  $45^\circ$  dichroic mirror which combines the trapping and the detector beams. Next, a 1:1 telescope provides manual control of the overall position of the entire multiple optical tweezers' pattern in the specimen plane. The combined laser beams are coupled into the microscope from the side, through a small dichroic mirror mounted directly below the dichroic filter cube used for epifluorescence (prototype optical trapping port, Nikon). This design enables the simultaneous use of fluorescence and optical tweezers, although care must to be taken in selecting the dichroic mirrors for epi-fluorescence to prevent interference problems. The objective turret of the microscope was removed to eliminate a 48% light loss in the Nikon optics, attributable to optical coatings (on the Wollaston prism and a lens) that reflected near-infrared light. This turret was replaced with a custom-built tube that holds an objective (100x/1.3 NA oil Plan Neofluar, Zeiss) and Wollaston prism for DIC imaging.

We require constant optical power delivered to the specimen whenever the laser beam is moved, either by the AOD's or the 1:1 positioning telescope. To achieve this, the two AOD's are placed as close together as possible. The plane in between these and the plane of the first lens of the 1:1 telescope are then optically imaged into the back aperture of the objective: beam-deflecting elements and the back aperture of the objective therefore lie in conjugate optical planes (blue colored elements, Fig. 5). Optical rotations of the beam in these planes produce corresponding translations of the spot in the specimen plane.

### E. The Position Detector

A polarized HeNe laser (1105P, 5 mW, Uniphase) supplies light to the position detector (green lines, Fig. 5). The power of the HeNe laser is sufficiently low that it does not trap particles yet sufficiently high to provide ample light for the photodetector. After beam expansion, an auxiliary 1:1 telescope is used for  $x$ - $y$  positioning of the detector spot, independent of the trapping light. A dichroic mirror then merges the red and infrared beams, after which they both pass through the main 1:1 telescope, which repositions both laser spots in the specimen plane simultaneously. After passing through both the specimen and condenser, the detector light is deflected from the microscope optical path by a  $45^\circ$  dichroic mirror, sent along a rigidified optical rail (mounted on the condenser system), then through a lens that images the back focal plane of the condenser onto a quadrant photodiode (SPOT9-DM1, UDT). The diode currents from each quadrant are converted to voltages by custom-built, two-stage preamplifiers. Preamp signals are passed to normalizing differential amplifiers that output separate  $x$ - and  $y$ -position voltages, which are then digitized by a 12-b multifunction A/D board (AT-MIO-16-E2, National Instruments).

### F. Position Detector Calibration

Since the detector and the tweezers are uncoupled, calibration of position becomes relatively easy and can be accomplished quickly for any particle trapped at any location within the field of view. Before detector calibration, one must perform one-time calibrations of both the video system and the AOD's. The video system is first calibrated by determining the correspondence between pixels and nanometers by imaging a ruled line pattern on the CCD camera (see dual-beam calibration, above). Next, a bead is trapped and moved back and forth along a diagonal (i.e., activating both  $x$  and  $y$  deflections) by driving the AOD's with periodic triangle waves over a preselected range of acoustic frequencies, while video-recording the movement on an optical-memory disc recorder (OMDR). Centroid tracking algorithms, which are accurate to the subpixel level [27], are then used to determine the response amplitude of the AOD's, in nm/MHz. Once these system-wide calibrations have been done, calibration of the photodetector can be performed straightforwardly: a trapped bead is once again moved back and forth diagonally over a known distance while the outputs of the photodiode sensor are recorded. The extremely high reproducibility of the AOD's allows averaging of detector output for 50 periods or more, thereby reducing the

effects of Brownian noise in the trap. The detector response to small displacements ( $\sim\pm 100$  nm) is quite linear, but the active range can be extended to about  $\pm 200$  nm by fitting the sensor output to a cubic (or higher order) polynomial.

## VI. TWO EXPERIMENTAL EXAMPLES

### A. Kinesin: A Molecular Motor

To study molecular motors, a variety of *in vitro* motility assays has recently been developed. In one form of these assays, used to study the motor protein kinesin, motors are attached to tiny beads which act as microscopic handles by which motors can be manipulated with an optical trap, as well as functioning as markers for scoring motor position during movement. Kinesin molecules in an extremely dilute suspension are nonspecifically adsorbed to the surfaces of beads  $\sim 0.5$   $\mu\text{m}$  in diameter, such that the beads carry from one to several motor molecules each. Microtubules, normally several micrometers in length but with a diameter of just 25 nm, are introduced to a microscope flow cell and become attached to the pretreated coverglass surface. Despite their small diameters, immobilized microtubules can be imaged individually by VE-DIC microscopy. A suspension of kinesin-coated beads is then introduced into the flow cell, in a buffer containing ATP. Optical tweezers are used to capture single diffusing beads and deposit these on the surface of a microtubule. The kinesin-coated beads bind to, and move along, microtubules for distances of a micrometer or thereabouts, analogous to the motion of vesicles inside living cells. Nanometer-scale measurements of bead displacements permit characterization of motor activity at the molecular level. Experiments of this type have already shown that kinesin takes molecular steps of  $\sim 8$  nm [7] and can work against loads of up to 5–6 pN [28].

Measurements of kinesin steps are most easily performed at low ATP concentrations, where the motion is diffusion-limited by the arrivals of ATP molecules and therefore radically slowed, making the stepwise transitions more apparent. The optical trap has the effect of increasing the stiffness acting on the bead, reducing its Brownian excursions to  $\sim 12$ – $25$  nm before filtering (the actual amount depends on the stiffness). Brownian noise also decreases with increasing force on the molecule, because the increased load stiffens the linkage between the kinesin and the bead, further increasing the system stiffness [7], [28].

Fig. 6 shows a data record of up to 25 or more steps visualized for a single molecule of kinesin moving along a microtubule *in vitro*, obtained with the time-sharing trapping system described above (for this purpose, only a single trap was generated). Since the kinesin-bead linkage has a finite compliance, the displacement of the bead reflects, but does not exactly equal, the displacement of the molecule itself, and a small but variable correction (typically  $\sim 15\%$  beyond forces of  $\sim 1$  pN) must be made for this effect. The trace clearly demonstrates the reduction in noise due to the change in series compliance that accompanies the increase in load as molecules move away from the trap center [7], [28].

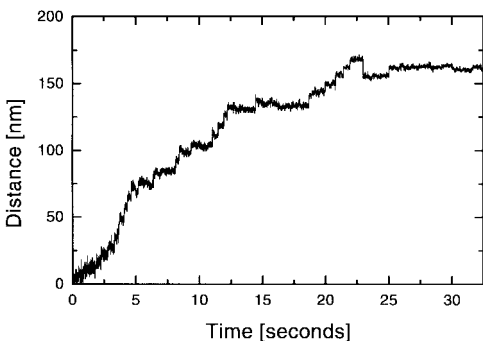


Fig. 6. Nanometer-scale measurement of the motion of a silica bead ( $0.5\text{-}\mu\text{m}$  diameter) produced by a single kinesin molecule moving along a microtubule. Data were recorded at 2 kHz, anti-alias filtered at 1 kHz, and median-filtered with a 13-point kernel (see text).

Microtubules are polar structures: they have a “plus” and a “minus” end. Kinesin motors move toward the plus end of microtubules (certain kinesin-related proteins, such as *ncd* and *KAR3*, move in the opposite sense). This directionality is certainly borne out in the records of individual molecules, but occasionally rearwards steps are observed, particularly at high loads (see Fig. 6 and [28]). This “slippage,” if that is the appropriate term, most likely does not correspond to a momentary detachment of the entire kinesin molecule, because the bead would be drawn back to the center of the trap almost immediately at loads of several piconewtons ( $\sim 5$  pN at 150-nm displacement, for the experiment shown in Fig. 6). Somehow, the molecule must slip without fully detaching, or perhaps execute true rearwards steps, reversing all or part of the mechanochemical cycle. Experiments are underway in our laboratory with both native kinesin and with recombinant derivatives of kinesin, aimed at shedding light on this and other interesting questions.

### B. Microtubule Stiffness

Multiple tweezers can be used to study the micromechanical properties of biological (and other) materials. Fig. 7 demonstrates the use of our dual-beam trap to bend a single microtubule. In the upper image, a straight (relaxed) microtubule is seen. Polystyrene beads ( $0.5\text{-}\mu\text{m}$  diameter) are attached to the microtubule near either end, and used as “handles” to capture and hold the microtubule by means of the two optical traps. As the traps are brought closer together by adjusting external controls, they transmit compressive forces to the microtubule through the two beads. Eventually, the microtubule buckles (Euler buckling). Since the displacement of beads from the trap centers at the moment of buckling can be measured, the force required to buckle a microtubule can be determined [15], [16]. The bending rigidity of a microtubule can be computed from this critical force. More accurate estimates of the bending rigidity can also be obtained from a detailed analysis of the shapes of bent microtubules under known load. The ability to measure elastic properties directly at the macromolecular level allows one to quantify, for example, how such properties might change during the cell cycle, or between different types of cells, or in the presence of various microtubule reagents and/or binding proteins.



(a)



(b)

Fig. 7. Buckling of a microtubule. (a) A single microtubule is held by two polystyrene beads trapped in each the twin beams of the dual-beam trap. (b) The traps are brought closer together, buckling the microtubule. Detailed analysis of the shape of the buckled microtubule and the applied force enables the determination of microtubule stiffness. Scale bar,  $2\ \mu\text{m}$ .

## VII. SUMMARY

We have described design features of two types of multiple-beam optical tweezers: a dual-beam trap and a time-sharing trap. Of the two, the time-sharing trap is clearly the more versatile, because of its capability to generate several beams and support a variety of feedback enhancements. However, it is comparatively more difficult to build and far more costly to produce. For many experiments, the dual-beam trapping scheme is simpler and more economical and may supply additional stability in some situations. Variants of the same quadrant photodiode-based position detection scheme are used in both setups, each capable of nanometer-level resolution. Optical tweezers, when combined with such position detectors, offers two important advances: the ability to manipulate molecular-scale objects, by means of attached bead “handles,” and the ability to measure directly forces and displacements on the molecular scale. Multiple traps, in particular, make possible experimental geometries not readily achieved with alternative technologies, such as scanning force microscopy (SFM) or glass microneedles. Moreover, the mechanical stiffness of an optical trap can be instantly changed, in contrast to these other approaches. Of particular importance are the noninvasive and

nondestructive character of optically based measurements, as well as the unparalleled spatial and temporal control afforded by the use of light. The use of optical tweezers is still relatively new in biology. It is also beginning to have a significant impact on other areas, including colloidal and polymer physics [29]–[32]. We anticipate continuing developments in these and related areas during the next few years and eagerly await the exciting advances that will surely result from the addition of this tool to the impressive arsenal of (bio)physical techniques.

#### ACKNOWLEDGMENT

The authors would like to thank M. Wang, M. Schnitzer, and S. Smith for helpful discussions, W. Ryu for the initial construction of the dual-beam trap, and W. Hill of the Rowland Institute for Science for electronics design and construction. The first author, K. Visscher, is a Burroughs-Wellcome Fellow of the Life Sciences Research Foundation.

#### REFERENCES

- [1] A. Ashkin, J. M. Dziedzic, J. E. Bjorkholm, and S. Chu, "Observation of a single-beam gradient force optical trap for dielectric particles," *Opt. Lett.*, vol. 11, pp. 288–290, 1986.
  - [2] A. Ashkin, J. M. Dziedzic, and T. Yamane, "Optical trapping and manipulation of single cells using infrared laser beams," *Nature*, vol. 330, pp. 769–771, 1987.
  - [3] A. Ashkin and J. M. Dziedzic, "Internal cell manipulation using infrared laser traps," *PNAS*, vol. 86, pp. 7914–7918, 1989.
  - [4] A. Ashkin, K. Schuetze, J. M. Dziedzic, U. Euteneuer, and M. Schliwa, "Force generation of organelle transport measured *in vivo* by an infrared laser trap," *Nature*, vol. 348, pp. 346–348, 1990.
  - [5] J. T. Finer, R. M. Simmons, and J. A. Spudich, "Single myosin molecule mechanics: Piconewton forces and nanometer steps," *Nature*, vol. 368, pp. 113–119, 1994.
  - [6] J. E. Molloy, J. E. Burns, J. Kendrick-Jones, R. T. Tregear, and D. C. S. White, "Movement and force produced by a single myosin head," *Nature*, vol. 378, pp. 209–212, 1995.
  - [7] K. Svoboda, C. F. Schmidt, B. J. Schnapp, and S. M. Block, "Direct observation of kinesin stepping by optical trapping interferometry," *Nature*, vol. 365, pp. 721–727, 1993.
  - [8] S. M. Block, D. F. Blair, and H. C. Berg, "Compliance of bacterial flagella measured with optical tweezers," *Nature*, vol. 338, pp. 514–518, 1989.
  - [9] A. Ashkin, "Forces of a single-beam gradient laser trap on a dielectric sphere in the ray optics regime," *Biophys. J.*, vol. 61, pp. 569–582, 1992.
  - [10] K. Svoboda and S. M. Block, "Biological applications of optical forces," *Annu. Rev. Biophys. Biomol. Struct.*, vol. 23, pp. 247–285, 1994.
  - [11] S. C. Kuo and M. P. Sheetz, "Force of single kinesin molecules measured with optical tweezers," *Science*, vol. 260, pp. 232–243, 1993.
  - [12] R. M. Simmons, J. T. Finer, S. Chu, and J. A. Spudich, "Quantitative measurements of force and displacement using an optical trap," *Biophys. J.*, vol. 70, pp. 1813–1822, 1996.
  - [13] M. D. Wang, H. Yin, R. Landick, J. Gelles, and S. M. Block, "Stretching DNA with optical tweezers," *Biophys. J.*, vol. 72, pp. 1335–1346, 1997.
  - [14] P. J. H. Bronkhorst, G. J. Streekstra, J. Grimbergen, E. J. Nijhof, J. J. Sixma, and G. J. Brakenhoff, "A new method to study shape recovery of red blood cells using multiple optical tweezers," *Biophys. J.*, vol. 69, pp. 1666–1673, 1995.
  - [15] M. W. Allersma, A. G. Z. Crowley, and C. F. Schmidt, "Bending of microtubules by applying calibrated forces with optical tweezers," *Biophys. J.*, vol. 68, p. A288, 1995.
  - [16] M. Kurachi, M. Hoshi, and H. Tashiro, "Buckling of a single microtubule by optical trapping forces: Direct measurement of microtubule rigidity," *Cell Mot. Cytoskel.*, vol. 30, pp. 221–228, 1995.
  - [17] H. Misawa, K. Sasaki, M. Koshioka, N. Kitamura, and H. Masuhara, "Multibeam laser manipulation and fixation of microparticles," *Appl. Phys. Lett.*, vol. 60, pp. 310–312, 1992.
  - [18] K. Visscher, G. J. Brakenhoff, and J. J. Krol, "Micromanipulation by multiple optical traps created by a single fast scanning trap integrated with the bilateral confocal scanning laser microscope," *Cytometry*, vol. 14, pp. 105–114, 1993.
  - [19] K. Sasaki, M. Koshioka, H. Misawa, N. Kitamura, and H. Masuhara, "Pattern formation and flow control of fine particles by laser-scanning micromanipulation," *Opt. Lett.*, vol. 16, pp. 1463–1465, 1991.
  - [20] M. M. Burns, J.-M. Fournier, and J. A. Golovchenko, "Optical matter: Crystallization and binding in intense optical fields," *Science*, vol. 249, pp. 749–754, 1990.
  - [21] A. Ashkin, "Feedback stabilization of optically levitated particles," *Appl. Phys. Lett.*, vol. 30, pp. 202–204, 1977.
  - [22] S. Kamimura, "Direct measurements of nanometric displacements under an optical microscope," *Appl. Opt.*, vol. 26, pp. 3425–3427, 1987.
  - [23] W. Denk and W. W. Webb, "Optical measurements of picometer displacements of transparent microscopic objects," *Appl. Opt.*, vol. 29, pp. 2382–2390, 1991.
  - [24] L. P. Ghislain and W. W. Webb, "Scanning-force microscope based on an optical trap," *Opt. Lett.*, vol. 18, pp. 1678–1680, 1993.
  - [25] L. P. Ghislain, N. A. Switz, and W. W. Webb, "Measurement of small forces using an optical trap," *Rev. Sci. Instrum.*, vol. 65, pp. 2762–2768, 1994.
  - [26] S. B. Smith, Y. Cui, and C. Bustamante, "Overstretching B-DNA: The elastic response of individual double-stranded and single-stranded DNA molecules," *Science*, vol. 271, pp. 795–799, 1996.
  - [27] J. Gelles, B. J. Schnapp, and M. P. Sheetz, "Tracking kinesin-driven movements with nanometer-scale precision," *Nature*, vol. 331, pp. 450–453, 1988.
  - [28] K. Svoboda and S. M. Block, "Force and velocity studied for single kinesin molecules," *Cell*, vol. 77, pp. 773–784, 1994.
  - [29] J. C. Crocker and D. G. Grier, "Microscopic measurement of the pair interaction potential of charge-stabilized colloid," *Phys. Rev. Lett.*, vol. 73, pp. 352–355.
  - [30] T. T. Perkins, D. E. Smith, R. G. Larson, and S. Chu, "Stretching of a single tethered polymer in a uniform flow," *Science*, vol. 268, pp. 83–87, 1995.
  - [31] T. T. Perkins, D. E. Smith, and S. Chu, "Direct observation of tube-like motion of a single polymer chain," *Science*, vol. 264, pp. 819–822, 1994.
  - [32] T. T. Perkins, S. R. Quake, D. E. Smith, and S. Chu, "Relaxation of a single DNA molecule observed by optical microscopy," *Science*, vol. 264, pp. 822–826, 1994.
- Koen Visscher**, photograph and biography not available at the time of publication.
- Steven P. Gross**, photograph and biography not available at the time of publication.
- Steven M. Block**, photograph and biography not available at the time of publication.